

# Microtubules self-repair in response to mechanical stress

Laura Schaedel<sup>1</sup>, Karin John<sup>2</sup>, Jérémie Gaillard<sup>1</sup>, Maxence V. Nachury<sup>3</sup>, Laurent Blanchoin<sup>1,\*</sup> and Manuel Théry<sup>1,4\*</sup>

1 – Laboratoire de Physiologie Cellulaire et Végétale, Institut de Recherche en Technologie et Science pour le Vivant, UMR5168, CEA/INRA/CNRS/UGA, Grenoble, France.

2- Laboratoire Interdisciplinaire de Physique, CNRS / UGA Grenoble 140 Rue de la Physique BP 87 - 38402 Saint-Martin-d'Hères, France

3- Department of Molecular and Cellular Physiology, Stanford University School of Medicine, CA 94305, USA.

4 - Unité de Thérapie Cellulaire, Hôpital Saint Louis, Institut Universitaire d'Hématologie, UMRS1160, INSERM/AP-HP/Université Paris Diderot, Paris, France.

Correspondence : [laurent.blanchoin@cea.fr](mailto:laurent.blanchoin@cea.fr), [manuel.thery@cea.fr](mailto:manuel.thery@cea.fr)

## Supplementary information

Supplementary figure S1 – S8

Supplementary video 1 – 6 legends

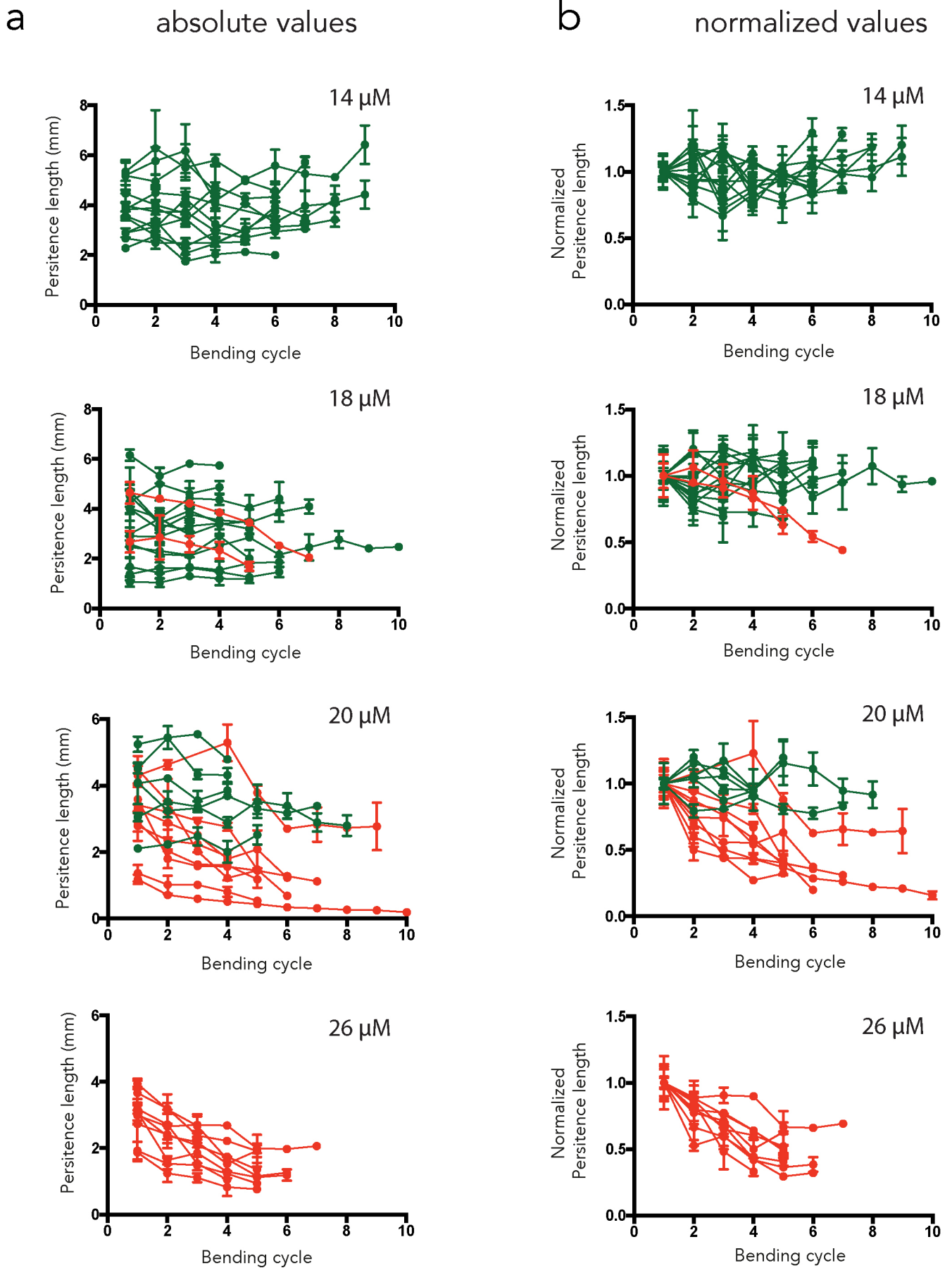
## Supplementary Figures

Supplementary Figure S1 - Measurements of microtubule persistent length evolution over the successive bending cycles.

a, Microtubules were grown in the presence of 14, 18, 20 or 26  $\mu\text{M}$  of tubulin and bent several times. Error bars correspond to the standard deviation calculated from 5 consecutive frames for each bending cycle. As a test of tendency, Spearman correlation tests for persistent length values over the successive cycles were performed. Green curves show microtubules for which the persistent length was not significantly affected over the bending cycles, whereas red curves show those that have been softened during the cyclic stress.

b, Same as a excepted that microtubule persistent lengths over bending cycles were normalized to their initial value.

Figure S1



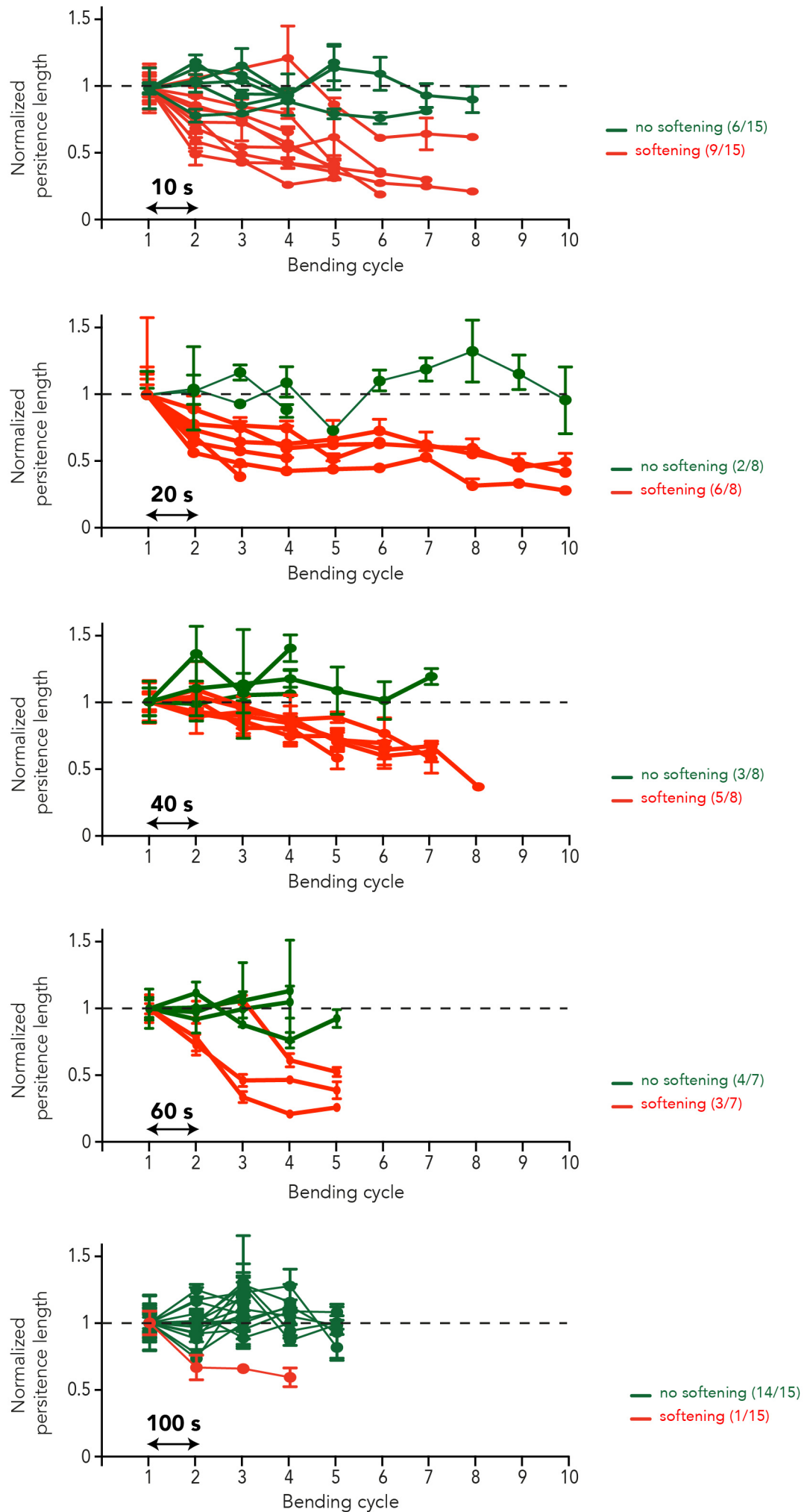
Supplementary Figure S2 – Impact of the delay between bending cycles on the evolution of microtubule persistent length.

Microtubules were grown in the presence 20  $\mu\text{M}$  of tubulin and bent several times. Delay between bending cycles was varied between 10 s (top line) and 100 s (bottom line). Microtubule persistent length was measured over the successive bending cycles. Microtubule persistent lengths were normalized to their initial value. Error bars correspond to the standard deviation calculated from 5 consecutive frames for each bending cycle. As a test of tendency, Spearman correlation tests for persistent length values over the successive cycles were performed. Green curves show microtubules for which the persistent length was not significantly affected over the bending cycles, whereas red curves show those that have been softened during the cyclic stress. The proportion of microtubules for which the persistent length decreased over the bending cycles reduced as the delay between the cycles was increased.



Figure S2

20  $\mu$ M tubulin



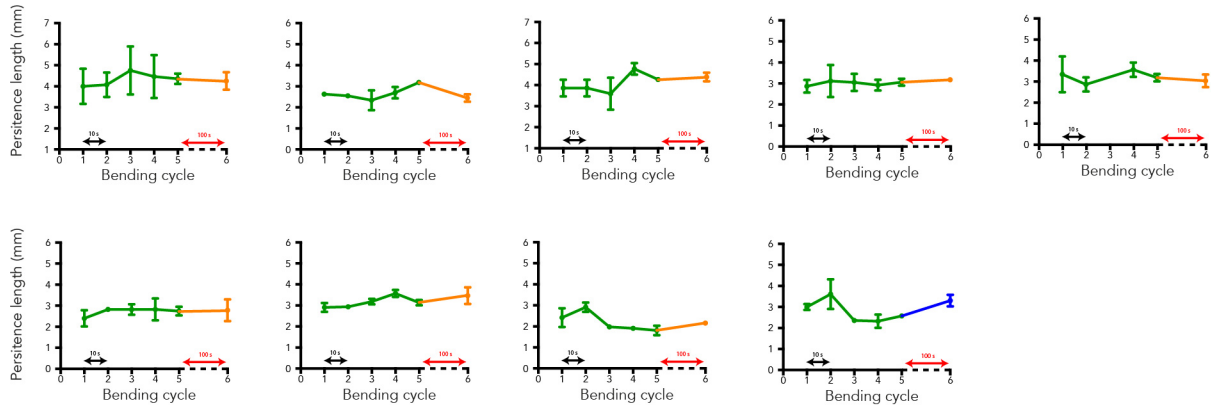
Supplementary Figure S3 - Evolution of microtubule persistent length following five rapid bending cycles.

Microtubules were grown in the presence 20  $\mu\text{M}$  of tubulin and bent five times with 10 s delay between the bending cycles. Then microtubules were not stimulated during 100 s. Stiffness recovery was measured by a last bending cycle after this rest period. To first distinguish softening from non-softening microtubules during the first bending cycles, we used the distance between the minimum normalized  $L_p$  and the  $L_p$  during the first cycle as a parameter for a k-means clustering. The clustering algorithm found one group with a low distance, which corresponds to non-softening microtubules (a, b), and another group with a high distance, corresponding to softening microtubules (c ,d). The recovery after a 100 s pause time was assessed by comparing  $L_p$  before and after the pause with a Wilcoxon matched-pairs test. Microtubules displaying significant recovery are shown in blue, the other in orange. No stiffness change could be observed in the group displaying no softening during the first bending cycles (a, b) whereas a significant stiffness increased was measured in a majority of microtubule that have been soften during the first bending cycles (c ,d).

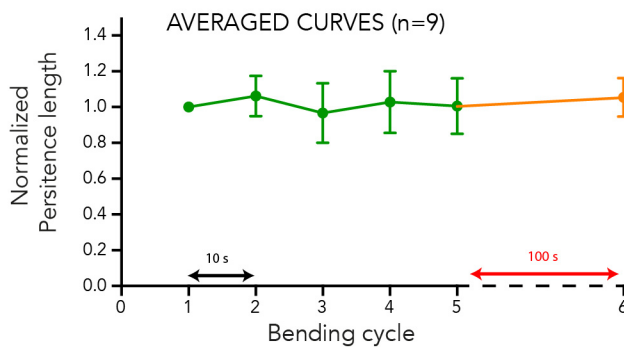
a, c, individual microtubule persistent length evolution during the five first bending cycles and the 100 s rest period.

b, d, average microtubule persistent length evolution during the five first bending cycles and the 100 s rest period.

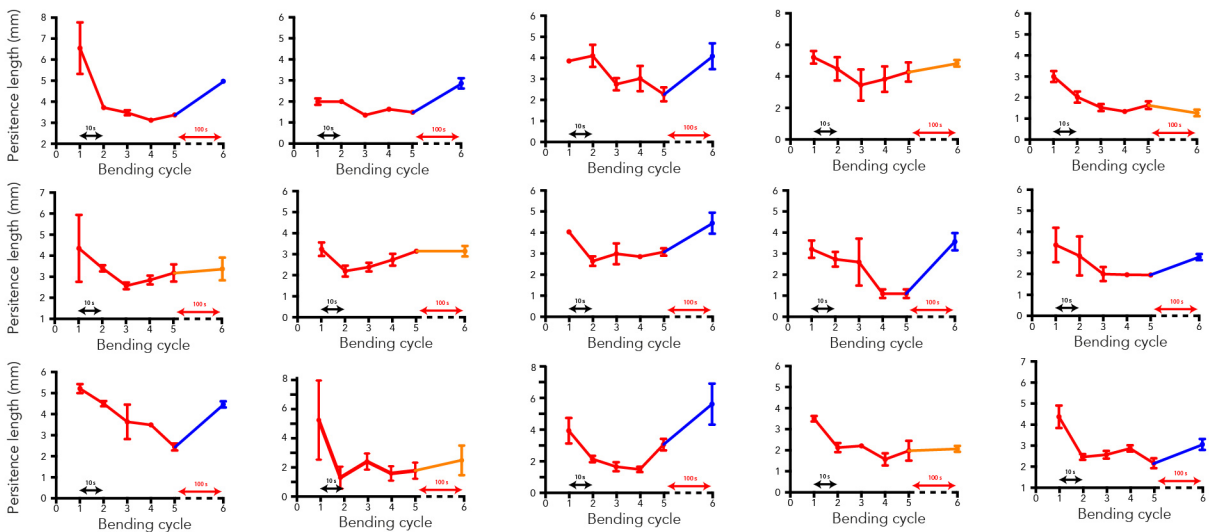
**a** Microtubules displaying NO significant softening during the 5 first rapid bending cycles



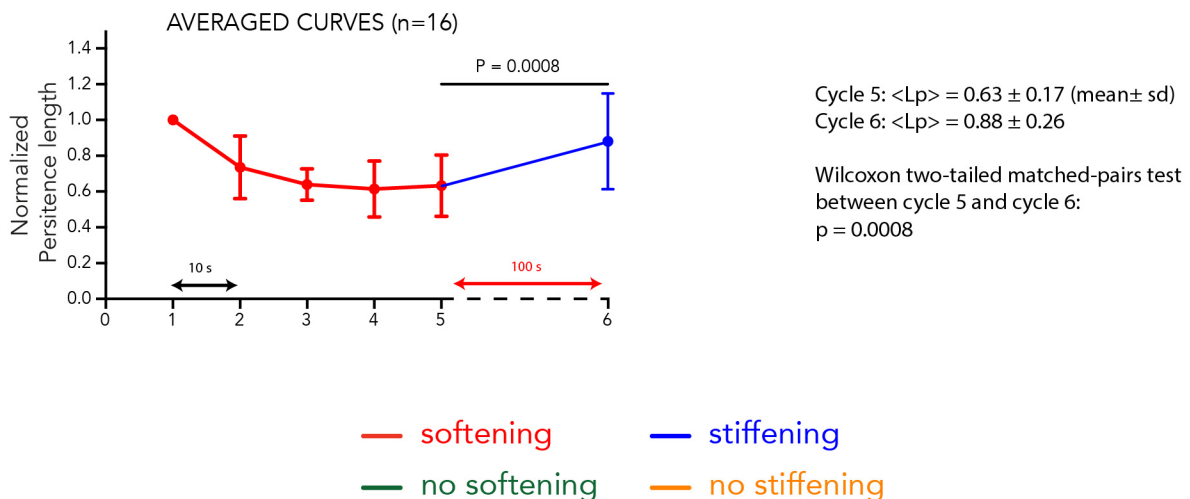
**b**



**c** Microtubules displaying a significant softening during the 5 first rapid bending cycles



**d**



Supplementary Figure S4 – Laser-induced damages in microtubule lattice.

A laser emitting pulses at 561 nm was used to damage microtubule lattice. The total energy was modulated by varying laser repetition rate.

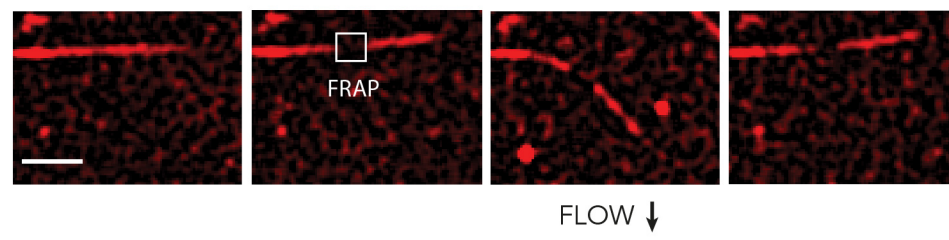
a, at low energy, microtubules were bleached but not damaged as revealed by the regular curved shapes they adopted when submitted to external flow.

b, at medium energy, microtubules were physically damaged, as shown by the kinked shape they displayed when submitted to flow. Microtubules were not severed and recovered their original straight shape as flow was stopped.

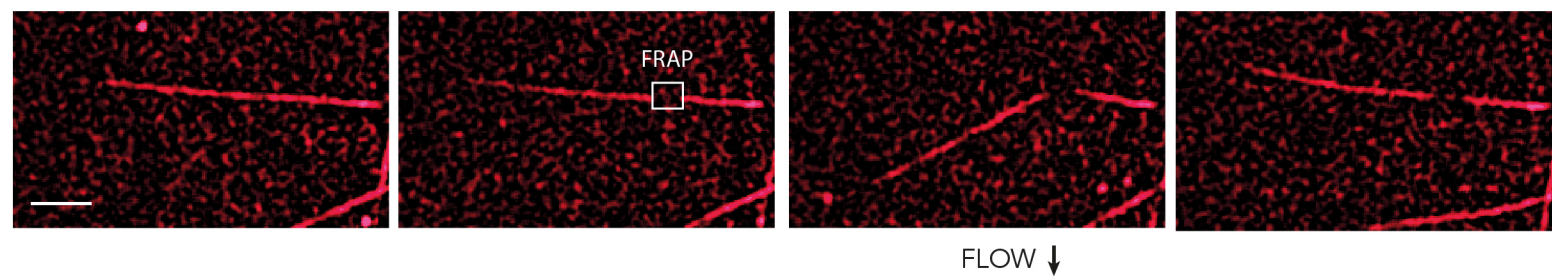
c, at high energy, microtubules were cut by the light pulses.

Figure S4

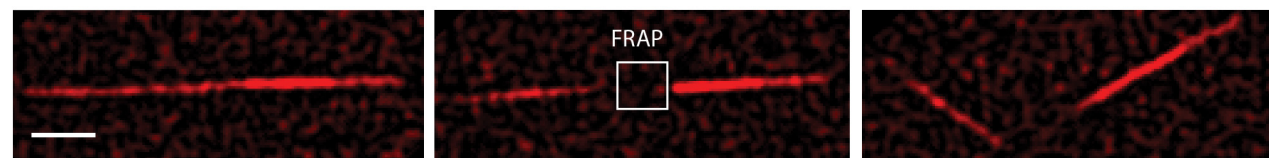
LOW POWER - microtubule bleaching



MEDIUM POWER - microtubule damaging



HIGH POWER - microtubule breaking

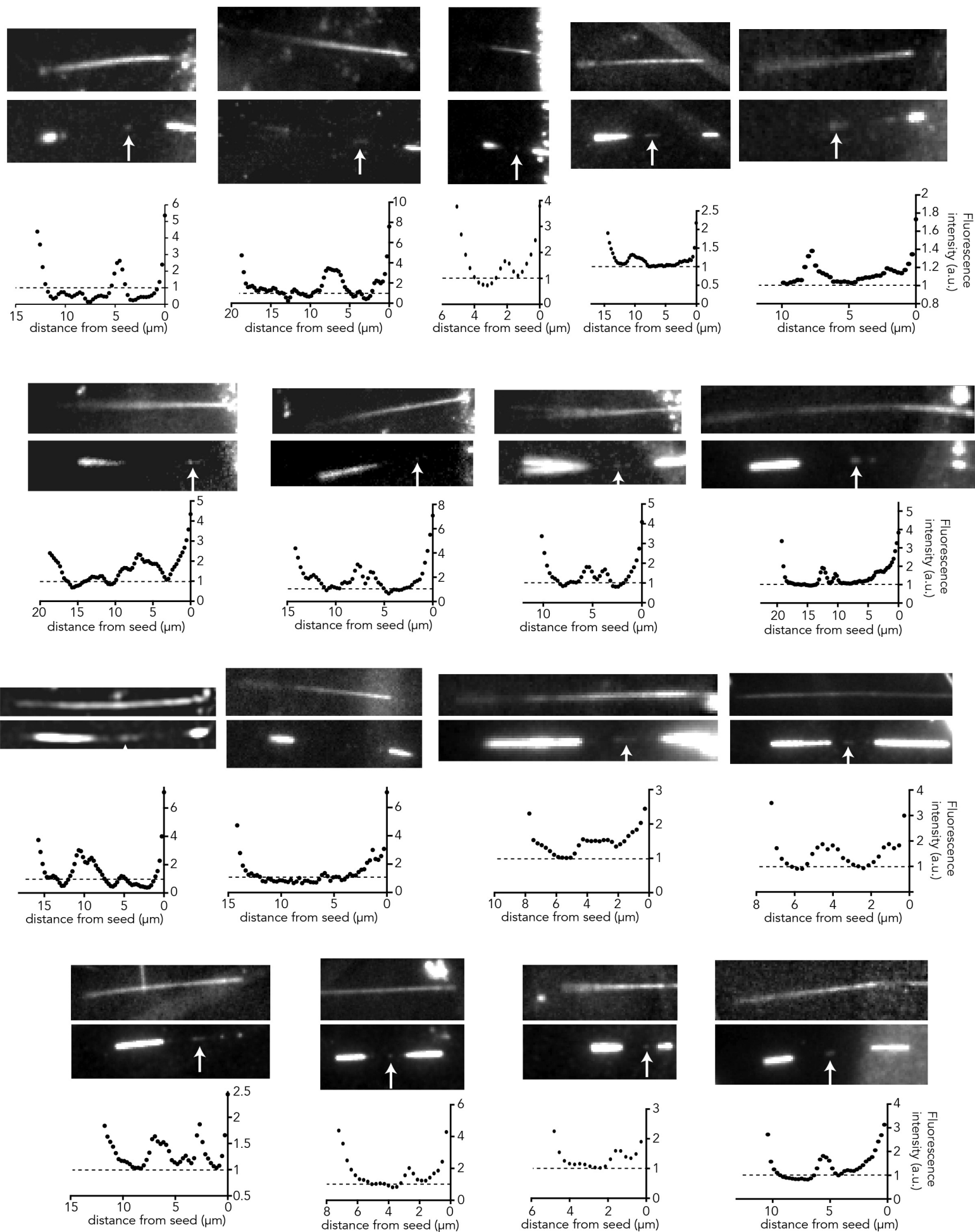


Supplementary Figure S5 – Examples of intra-lattice dimer incorporation in bent microtubules.

Seventeen examples of red fluorescent microtubules after five successive bending cycles in the presence of green tubulin. Upper pictures show red fluorescent channel, lower pictures show the green channel after fluorescent tubulin washout. Arrows point at incorporation sites of green dimers into the red lattice between the microtubule seed on the right and the growing end on the left. Graphics display the corresponding green fluorescence intensity linescan along microtubule length.

Figure S5

20  $\mu\text{M}$  tubulin



Supplementary Figure S6 – Examples of absence of intra-lattice dimer incorporation in non-bent microtubules.

a, Experimental procedure to grow microtubules with red tubulin and flow green tubulin along their length.

b, Nine examples of red fluorescent microtubules submitted to green tubulin flow along their length. Upper pictures show red fluorescent channel, lower pictures show the green channel after fluorescent tubulin washout. Graphics display the corresponding green fluorescence intensity linescan along microtubule length and show no intra-lattice incorporation along microtubule length.



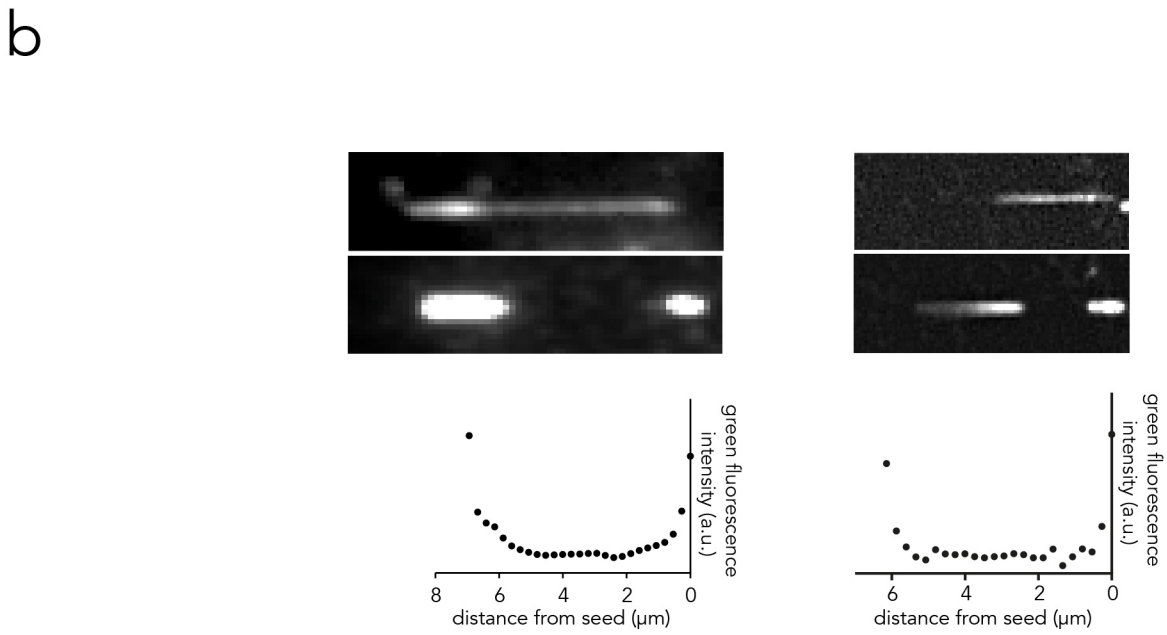
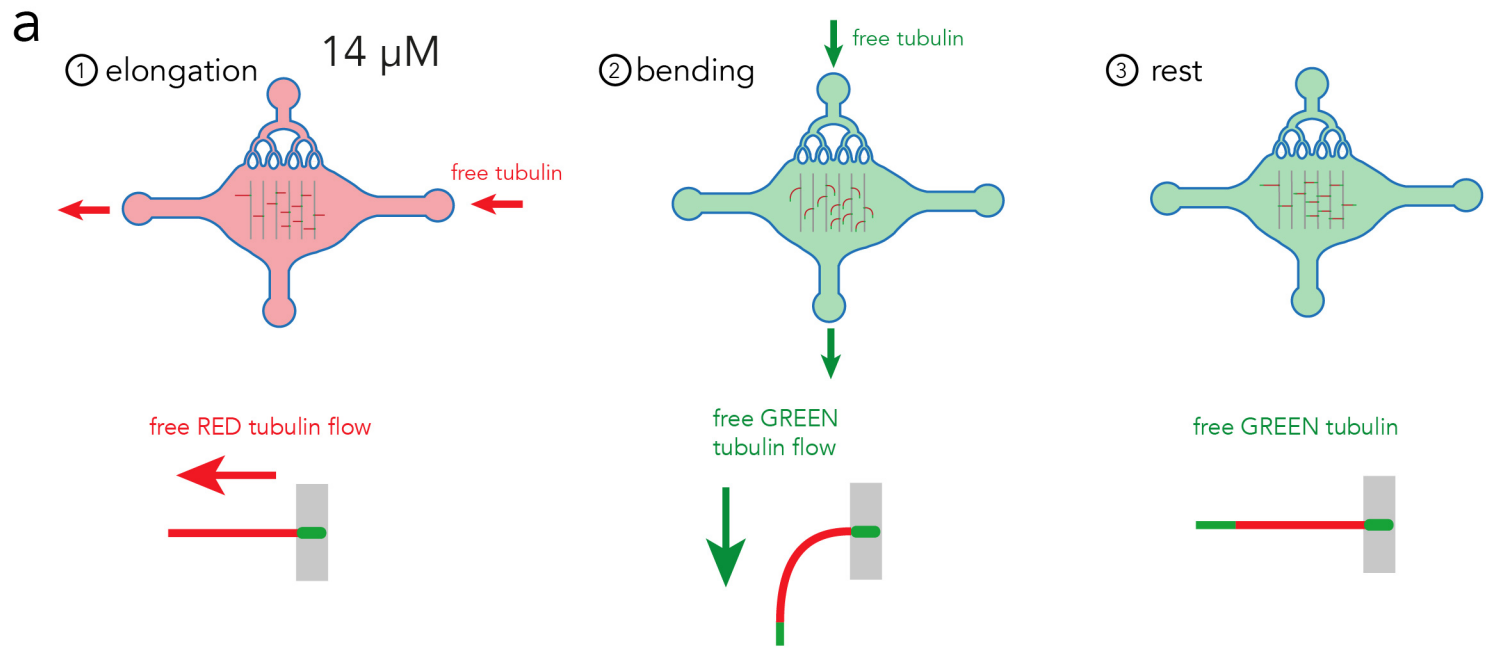


Supplementary Figure S7 – Examples of absence of intra-lattice dimer incorporation in slowly-assembled microtubules after successive bendings.

a, Experimental procedure to grow microtubules with 14  $\mu\text{M}$  of red tubulin and bend them in the presence of 20  $\mu\text{M}$  of green tubulin.

b, two examples of slowly-assembled red fluorescent microtubules after five successive bending cycles in the presence of green tubulin. Upper pictures show red fluorescent channel, lower pictures show the green channel after fluorescent tubulin washout. Graphics display the corresponding green fluorescence intensity linescan along microtubule length and show no intra-lattice incorporation along microtubule length.

Figure S7



Supplementary Figure S8 – Numerical simulations of microtubule bent shapes.

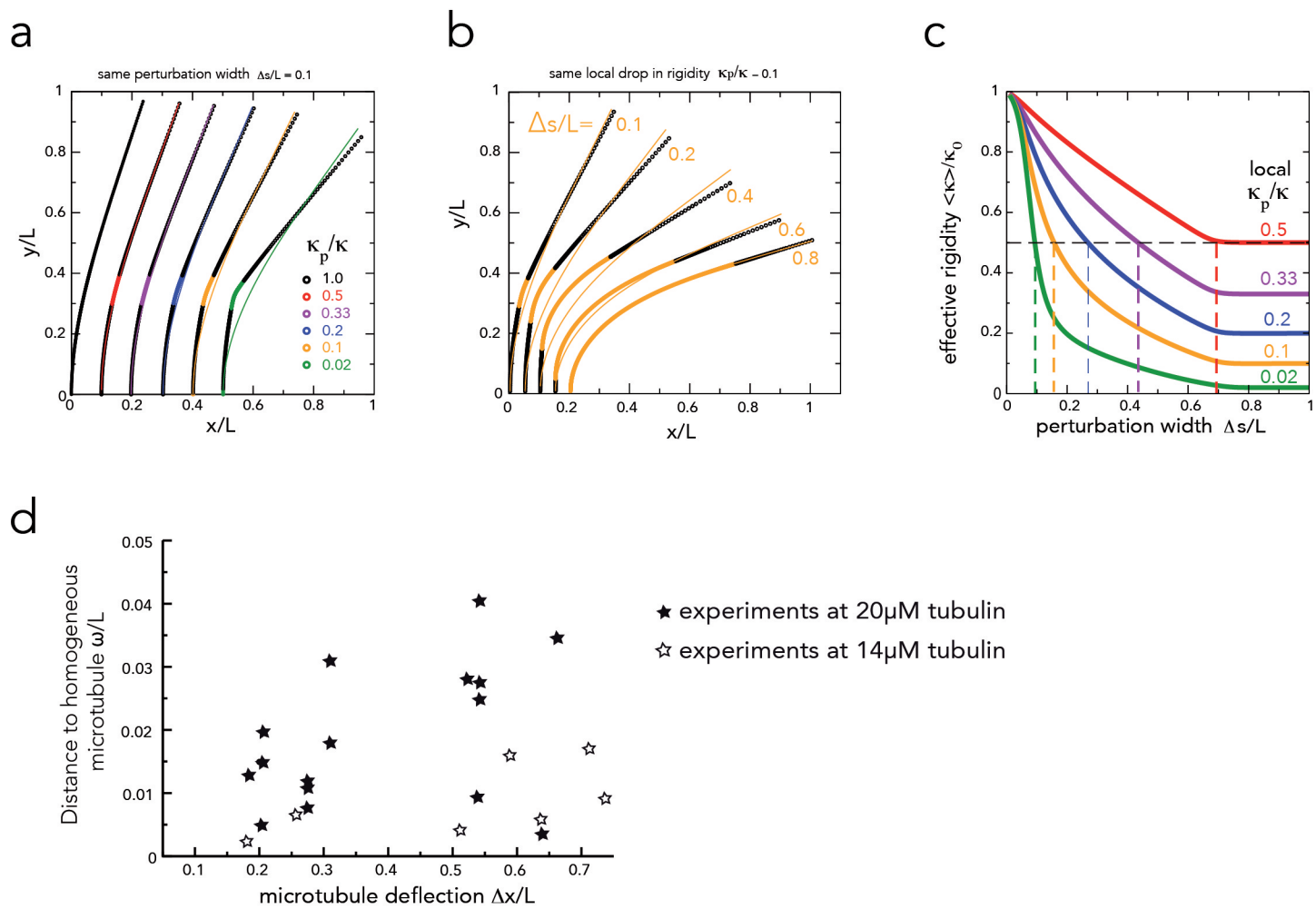
a, The graph shows the variations in the microtubule equilibrium shapes in response to a given hydrodynamic flow upon varying the stiffness reduction  $\kappa_p/\kappa_0$  over a short (10%) portion of the microtubule.

b, The graph shows the variations in the microtubule equilibrium shapes in response to a given hydrodynamic flow upon varying the width of the portion whose stiffness has been reduced 10 times.

c, The graph shows the variations of apparent average stiffness depending on the degree of local softening ( $\kappa_p/\kappa_0$ ) and the width on which it is applied ( $\Delta s/L$ ). A given effective rigidity can be obtained for distinct degrees ( $\kappa_p/\kappa_0$ ) and width ( $\Delta s/L$ ) of local softenings (as shown with dotted lines).

d, Comparison of the distances to numeric homogeneous microtubules for experimental observations of microtubules assembled at low and high concentrations of tubulin. The distance ( $\omega/L$ ) was plotted against microtubule deflection ( $\Delta s/L$ ) (see Figure 5c). Hollow stars correspond to microtubules assembled in the presence of 14  $\mu\text{M}$  of free tubulin. Full stars correspond to microtubules assembled in the presence of 20  $\mu\text{M}$  of free tubulin. Both were submitted to five bending cycles. Microtubules assembled in the presence of 14  $\mu\text{M}$  of free tubulin, and presumably with less lattice defects showed lower deviation to numeric and homogenous microtubules than microtubules assembled more rapidly in the presence of 20 $\mu\text{M}$  of free tubulin.

Figure S8



## Supplementary Videos

### Supplementary video 1

Time lapse sequence of microtubule (green) bending in response to fluid flow. Flow was applied during 10s (from  $t=10$  to  $t=20$ s). Red beads were added to the medium to measure fluid flow. Images were taken every 150 ms. Time display is min:sec.

### Supplementary video 2

Time lapse sequence of microtubule (green) bending in response to ten successive applications of fluid flow.

Flow sequences were applied during 10s every 20s. Red beads were added to the medium to measure fluid flow. Images were taken every 150 ms. Time display is min:sec.

### Supplementary video 3

Time lapse sequence illustrating microtubule lattice damaging with a pulsed laser. Microtubule was assembled from a micropatterned line and damaged with a laser pulse (red disc 1s after movie start) whose location was indicated with a red arrow in the few following images. Damaged microtubule was then submitted to a bending cycle after which it recovered its original straight shape; thereby confirming it was neither severed nor heavily damaged.

### Supplementary video 4

Time-lapse sequence illustrating a red microtubule damaged with a pulsed laser in the presence of green tubulin.

The microtubule was assembled from a micropatterned line with red tubulin, bathed in a solution of green tubulin ( $t=-3:20$ ), damaged (but not cut) with laser pulses ( $t=0$ ) and let in the presence of green tubulin (until  $t=1:30$ ). Green tubulin was washed away and replaced by red tubulin. Removal of the green fluorescent background revealed incorporation of tubulin dimers at the damaged site. The light excitation of the green fluorescence was increased at  $t=2:45$  to improve the visualization of the incorporated green tubulin. The light excitation of the red fluorescence was increased at  $t=3:15$  to highlight the red microtubule shaft.

### Supplementary video 5

Time-lapse sequence showing a red microtubule (red channel shown on the right) bent 5 times in the presence of green tubulin (green channel shown on the left). Green tubulin was washed out after 90 s and replaced by red tubulin. The light excitation of the green fluorescence was increased at  $t=171$  s to improve the

visualization of the incorporated green tubulin. Several sites of green tubulin incorporation were visible along microtubule length.

#### Supplementary video 6

Time lapse sequence showing a red microtubule (red channel shown on the right) submitted to flow along it in the presence of green tubulin (green channel shown on the left). Green tubulin was washed out after 140 s and replaced by red tubulin. The light excitation of the green fluorescence was increased at  $t=210$  s to improve the visualization of the incorporated green tubulin. No incorporation could be visualized along the microtubule length in those conditions.